Neuro-Oncology Advances
2(1), 1–13, 2020 | doi:10.1093/noajnl/vdaa043 | Advance Access date 28 March 2020

Interferon-β exposure induces a fragile glioblastoma stem cell phenotype with a transcriptional profile of reduced migratory and MAPK pathway activity

Birthe Lohmann, Manuela Silginer, Daniel Picard, Hannah Schneider, Marc Remke, Patrick Roth, Guido Reifenberger, and Michael Weller

Laboratory of Molecular Neuro-Oncology, Department of Neurology, University Hospital and University of Zurich, Zurich, Switzerland (B.L., M.S., H.S., P.R., M.W.); Division of Pediatric Neuro-Oncogenomics, German Cancer Research Center (DKFZ), Heidelberg, Germany (D.P., M.R.); German Consortium for Translational Cancer Research (DKTK), Partner Site Essen/Düsseldorf, Düsseldorf, Germany (D.P., M.R., G.R.); Department of Pediatric Oncology, Hematology, and Clinical Immunology, Medical Faculty, University Hospital Düsseldorf, Düsseldorf, Germany (D.P., M.R.); Institute of Neuropathology, Medical Faculty, Heinrich-Heine University Düsseldorf, Düsseldorf, Germany (D.P., M.R., G.R.)

Corresponding Author: Michael Weller, MD, Department of Neurology, University Hospital and University of Zurich, Zurich, Switzerland (michael.weller@usz.ch).

Abstract

Background. Type I interferons (IFN-α/β) are cytokines that are typically expressed in response to double-stranded RNA associated with viral infections. Glioblastomas are the most common malignant primary brain tumors, characterized by an infiltrative growth pattern and prominent angiogenic activity, and thought to be maintained by a subpopulation of glioma-initiating (stem-like) cells (GICs). The growth of human GIC lines is highly sensitive to IFN-β.

Methods. Repetitive pulse stimulation with IFN-β1a (IS) was used to generate IS sublines that had acquired resistance to IFN-β-induced suppression of sphere formation. These cell lines were characterized by analyses of type 1 IFN signaling, growth patterns, and transcriptomic profiles.

Results. Here we report that repetitive IFN-β1a stimulation (IS) induces a stable phenotype (referred to as IS) at the level of maintaining sphere formation, although classical IFN signaling defined by the expression of both IFN receptors, myxovirus resistance protein A (MxA) accumulation, and STAT1 induction is unaffected. Furthermore, this stably altered IS phenotype is characterized by constitutively decreased sphere formation capacity and morphological features of senescence and autophagy. Transcriptional profiling reveals increased type I IFN signaling in these IS cells, but decreased expression of genes involved in receptor signaling and cell migration.

Conclusions. Altogether, these data suggest a role for promoting IFN-β signaling in glioblastoma and might provide clues to design future therapeutic approaches.

Key Points

- Repetitive exposure to IFN-β induces an IS phenotype characterized by acquired resistance to IFN-β-induced suppression of sphere formation despite preserved canonical type I IFN signaling.
- IS cells exhibited decreased growth and spherogenicity and a transcriptional profile of reduced migratory and MAPK pathway activity.

Importance of the Study

Type I interferons (IFN-α/β) contribute to the natural immune response to viral infections, but have also recently been attributed to anticancer stem stell properties. Glioblastomas are thought to be maintained by a subpopulation of glioma-initiating (stem-like) cells (GICs). The growth of human GIC lines is highly sensitive to IFN-β. We report that repetitive pulse exposure to IFN-β1a induces acquired resistance to IFN-β-induced suppression of sphere formation in GICs, despite preserved canonical type I IFN signaling (IS phenotype). Yet, IS GIC lines exhibit a fragile phenotype characterized by constitutively decreased spherogenicity, features of senescence, and a transcriptional profile of decreased expression of genes involved in receptor signaling and cell migration. These data suggest a role for promoting IFN-β signaling in the treatment of glioblastoma.

Glioblastomas without mutations in the isocitrate dehydrogenase (IDH) 1 or 2 genes, ie, IDH-wildtype glioblastomas are the most common and most malignant group of glial tumors. These tumors are characterized by a brain-infiltrative growth pattern, prominent angiogenic activity, and variable patterns of molecular genetic changes in signaling and cell cycle-related pathways.[1] IDH-wildtype glioblastoma patients have a poor prognosis with median survival in the range of 12 months in population-based studies[2,3] and of 14–17 months in contemporary clinical trials.[4–6] Besides surgery and radiotherapy, alkylating agent chemotherapy with temozolomide (TMZ) constitutes the standard treatment.[7,8] For at least two-thirds of the patients, the DNA repair protein O^6-methylguanine-DNA methyltransferase antagonizes the effect of TMZ.[9,10] To overcome this challenge, interferon (IFN)-β1a treatment is of interest since it may sensitize human glioma cells, including glioma-initiating cells (GICs), to irradiation and TMZ.[11,12]

IFNs are pleiotropic cytokines that are divided into 3 classes. Type I IFNs are a multi-member cytokine family consisting of around 20 members. The human genome contains genes encoding IFN-α (13 subtypes), IFN-β, IFN-ε, IFN-κ, and IFN-ω. They signal via the Janus-associated kinase–signal transducer and activator of transcription (JAK-STAT) cascade by binding to their cognate IFN-α/β receptor (IFNAR), IFNAR1 and IFNAR2. IFNAR1 associates with tyrosine kinase 2 and IFNAR2 with JAK1. This ligation leads to autophosphorylation of STAT members that translocate to the nucleus where they initiate transcription by binding specific sites in the promoter region of IFN-stimulated genes.[13] Type I IFNs control innate and adaptive immunity as well as intracellular antimicrobial programs. They limit the dissemination of infectious agents like viral pathogens by the induction of an antimicrobial state in infected cells and their neighboring cells. They also modulate the immune system by promoting antigen presentation and natural killer cell function while suppressing pro-inflammatory pathways and cytokine production. Furthermore, type I IFNs activate the adaptive immune system and thereby promote the development of T- and B-cell responses and immunological memory.[13–15] In addition, there is a growing body of evidence suggesting that type I IFNs are also involved in natural and therapy-induced immunological control of malignancies that are not virus-related. However, the exact role of the type I IFN-mediated immune response to cancer is not fully understood.[16] Different studies indicate that type I IFNs are involved in immunoediting,[17,18] a process in which the immune system protects the host against oncogenesis and is able to recognize and respond to tumor development.[19] Furthermore, IFN-α/β have been proposed to mediate antitumoral effects, which are often delayed but enduring, by acting on cancer stem cells.[20,21]

Type I IFNs have been investigated for the treatment of multiple neoplasms, eg, Kaposi sarcoma,[22] hairy cell leukemia,[16,23,24] renal cell carcinoma,[25] chronic myeloid leukemia,[26] and multiple myeloma.[27,28] Type I IFNs were also tested in phase I/II clinical trials that suggested potential activity in newly diagnosed glioblastoma,[29–31] yet, a recent randomized trial failed to confirm the activity of type I IFN when added to the standard of care in newly diagnosed glioblastoma.[32]

Resistance to conventional treatments like radio- and chemotherapy is considered a typical feature of GICs. Based on the establishment of models of acquired resistance to TMZ[33] and the profound anti-GIC properties of type I IFNs,[11] the present study explores the phenotypical changes and the underlying signaling perturbations caused by acquired resistance of GIC models to IFNs. Here we report that, while such IFN resistance can indeed be induced, it comes at a price of a stable change in phenotype referred to here as "IFN-stimulated" (IS) that is characterized by impaired tumor growth in vitro and in vivo, features of senescence and profound changes in gene expression related to receptor kinase signaling and cell migration.

Material and Methods

Materials and Cell Lines

Human IFN-β1a and pegylated IFN-β1a were provided by Biogen Inc. Stock solutions for in vitro experiments were prepared in 20 mM sodium acetate, pH 8.4, containing 150 mM arginine hydrochloride; 3-methyladenine was from Sigma Aldrich. After informed consent and approval of the local ethics committees, the GIC lines were established from freshly resected tumors as described previously.[34] Cells were cultured in phenol red-free Neurobasal medium (NB) with B-27 supplement (20 µL/mL) (ThermoFisherScientific), L-glutamine (10 µL/mL),

fibroblast growth factor-2, and epidermal growth factor (20 ng/mL each; Peprotech). TMZ was provided by Merck. All cells were regularly tested for mycoplasma contamination and sent for short tandem repeat analysis (Deutsche Sammlung von Mikroorganismen and Zellkulturen—DSMZ).

Generation of IFN-β1a-Resistant GICs

Samples of T-325, ZH-161, ZH-305, and S-24 cells were divided into 2 fractions indicated as GIC-NC for normal control GIC, which were not pulsed with IFN-β1a, or GIC-IS for GIC, which were serially stimulated with IFN-β1a. Both cell fractions were continuously processed in parallel. These models were passaged in NB medium without or with IFN-β1a at the same time intervals. IS cells underwent serial IFN-β1a stimulation with 10 IU/mL for T-325 and 100 IU/mL for ZH-161, ZH-305, and S-24 every 3–4 weeks. After completion of more than 4 stimulation rounds, a subfraction of NC and IS cells were separated and seeded to assess their clonogenic potential using spherogenicity assays. The remaining IS cells were kept in culture under permanent IFN-β1a stimulation as described above.

Real-Time PCR, Immunoblot, PCR and Viability Assay

Detailed methods are provided in Supplementary Note 1.

Gene Expression Profiling

About 500 ng total RNA was processed using the TruSeq RNA Sample Preparation v2 Kit (low-throughput protocol; Illumina) to prepare the barcoded libraries. Libraries were validated and quantified using DNA 1000 and high-sensitivity chips on a Bioanalyzer (Agilent); 7.5 pM denatured libraries were used as input into cBot (Illumina), followed by deep sequencing using HiSeq 2500 (Illumina) for 101 cycles, with an additional 7 cycles for index reading. Fastq files were imported into Partek Flow (Partek). Quality analysis and control were performed on all reads to assess read quality and to determine the amount of trimming required (both ends: 13 bases 5′and 1 base 3′). Trimmed reads were aligned against the hg38 genome using the STAR—v2.5.3a aligner. Unaligned reads were further processed using Bowtie 2 v2.2.5 aligner. Aligned reads were combined before quantifying the expression using the Partek Expectation-Maximization algorithm against the ENSEMBL (release 84) database. Finally, statistical gene set analysis was performed using the *T*-test to determine differential expression at the gene level. Partek flow default settings were used in all analyses. For pathway analysis, gene sets were derived from curated pathways from several databases including GO, Reactome, KEGG (August 01, 2018 version; http://download.baderlab.org/EM_Genesets/current_release/Human/symbol/) and visualized using Cytoscape (www.cytoscape.org; $P \leq .001$, $q \leq 0.05$, similarity cutoff 0.5). RNA sequencing data were analyzed by cell line IS versus NC, and the *T*-value was used to perform a ranked analysis.

Animal Studies

The standard operating procedures for the animal studies were approved by the Swiss Cantonal Veterinary Office under the Animal license permission number ZH105/2015. The care and treatment of all animals were in accordance with the Swiss Federal Law on the Protection of Animals of the Federal Food Safety and Veterinary Office and with the Swiss Federal Ordinance on the Protection of Animals. Following anesthesia, a burr hole was drilled in the skull 2 mm lateral to the bregma. The needle of a Hamilton syringe (Hamilton) was introduced to a depth of 3 mm. A single-cell suspension of 10^5 GICs in 2 μL PBS was slowly injected into the right striatum of immuno-compromised CD1 Foxn1 nude mice (Charles River) (n = 10 per group). The mice enrolled had body weights of more than 20 g. Systemic treatment with human peg-IFN-β1a was performed by subcutaneous injection twice weekly (8×10^7 U/kg). The mice were observed daily and euthanized by cervical dislocation when developing neurological symptoms or at defined time points for histological analysis as indicated. Three mice per group were euthanized, defined by a pre-randomized list, when the third mouse in any group of the experiment became symptomatic in order to perform histological analysis to assess tumor growth at an early stage. The remaining mice were euthanized when displaying neurological symptoms to obtain survival data. All brains were explanted upon euthanasia, embedded in cryo-moulds in Shandon Cytochrome yellow (Thermo Fisher Scientific) and frozen in liquid nitrogen. Tumor incidences and volumes were determined using hematoxylin and eosin stainings of 8 μm thick cryosections cut using a Microm HM560 (Microchom HM560, Thermo Scientific).[35] Details on immunohistochemistry methods are provided in Supplementary Note 2.

Data Analysis

Data are representative of experiments performed 2–3 times with similar results. Statistical analysis was performed using GraphPad Prism 5 or 7 software. Statistical significance was assessed using either two-sided unpaired and paired Student's *t*-test or one-way ANOVA with Tukey's post hoc test for multiple analyses. Quantitative data are represented as mean ± standard deviation (SD) or standard error of the mean (SEM). A *P*-value below .05 was considered significant. Kaplan–Meier survival curves generated from the animal studies were analyzed using the Gehan–Breslow–Wilcoxon test. A *P*-value below .05 was considered significant.

Results

Repeated Exposure to IFN-β1a Induces Resistance in GICs

To model acquired resistance to IFN-β1a in GIC in vitro, T-325, ZH-161, ZH-305, or S-24 cells underwent serial IFN-β1a stimulation every 3–4 weeks (Figure 1A). To ascertain the induction of a stable, IFN-β1a-resistant phenotype, we determined clonogenic survival and assessed the half-maximal effective

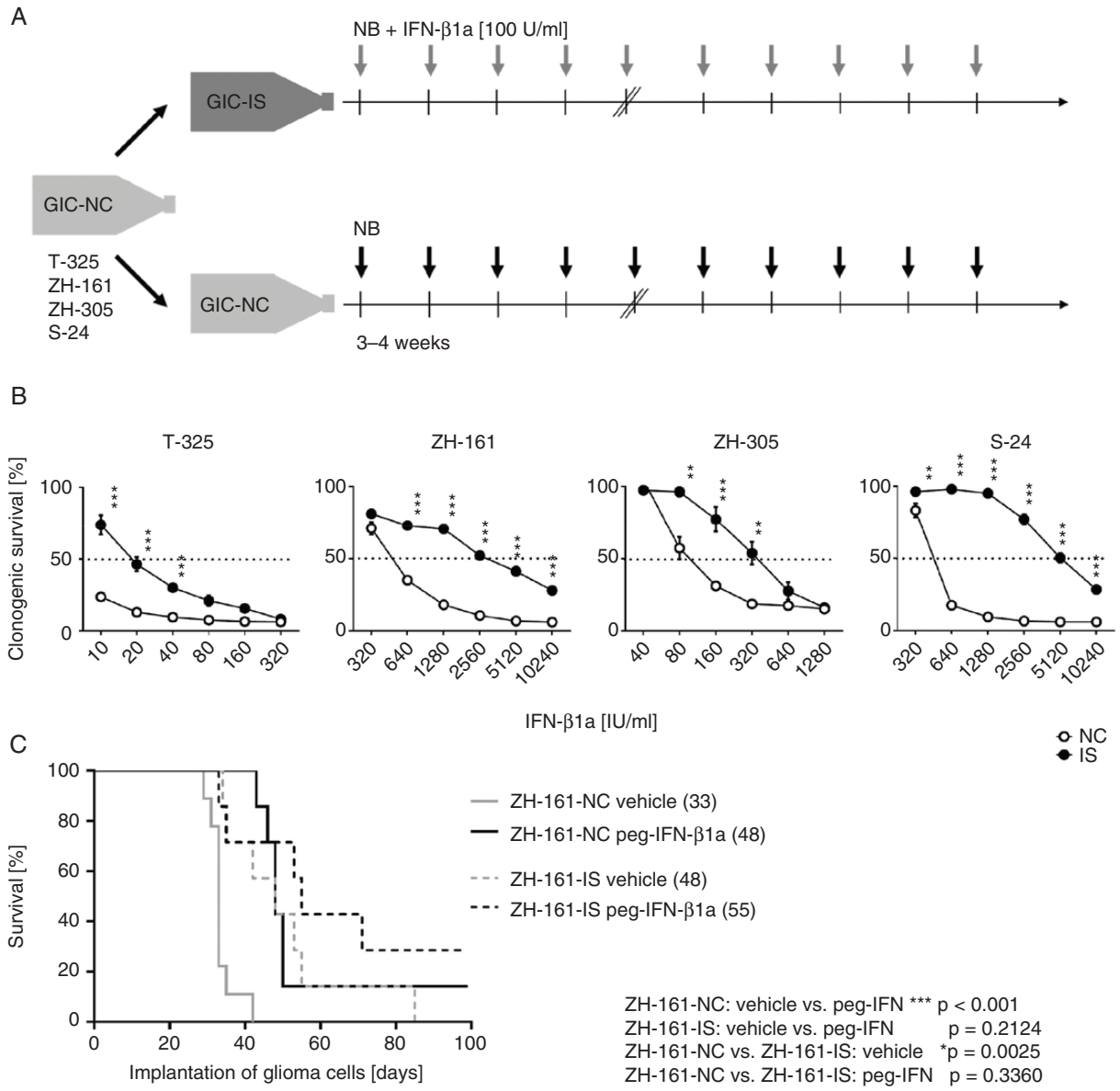

Figure 1. Responsiveness to IFN-β1a in normal control (NC) and interferon-stimulated (IS) cells in vitro. (A) Schematic illustration of the generation of IS cells. (B) Clonogenic survival of NC or IS cells upon IFN-β1a stimulation was assessed by MTT assay. (C) Nude mice intracranially implanted with ZH-161-NC or ZH-161-IS cells were treated twice weekly with vehicle or peg-IFN-β1a (8×10^7 U/kg) from day 14 on. Kaplan–Meier survival curves of ZH-161-NC or ZH-161-IS glioma-bearing mice are shown (median survival in days provided in brackets, Gehan–Breslow–Wilcoxon test, $P < .05$, $n = 7$–8 mice per group).

concentration (EC_{50}) of IS versus NC cells by metabolic activity assays. We noted an up to 8-fold increase of the EC_{50} values in IS cells (Figure 1B). This resistance phenotype was maintained in all 4 IS lines (T-325-IS, ZH-161-IS, ZH-305-IS, and S-24-IS) for 12 weeks after the last exposure to IFN-β1a. Later time points were not explored. Representative studies are shown in Supplementary Figure S1A. Next, ZH-161-NC or ZH-161-IS cells were orthotopically implanted into nude mice that were treated biweekly with peg-IFN-β1a or vehicle control to explore whether IFN resistance established in vitro is maintained in vivo. First, we noted that there were more longer surviving mice in the untreated ZH-161-IS than in the untreated ZH-161-NC groups. Moreover, treatment with peg-IFN-β1a prolonged survival in ZH-161-NC glioma-bearing mice (***P = .0001), but not in mice harboring ZH-161-IS gliomas (P = .2712) (Figure 1D).

Classical Type I IFN Signaling Is Not Affected in GIC-IS Cells

We next explored the level of signaling at which resistance to IFN-β1a had evolved in IS cells. Both cognate receptors, IFNAR1 and IFNAR2, were expressed on NC and IS cells on

mRNA (Figure 2A and B) and protein level (Figure 2C and D). Responsiveness to IFN-β1a was confirmed at the level of induction of STAT1 mRNA expression (Figure 2E). MxA as the classical downstream target of the IFN signaling cascade was also concentration-dependently induced at the mRNA (Figure 2F) and protein levels (Figure 2G) in NC and IS cells. The maintained signaling response to IFN was confirmed by a significant upregulation of MxA protein using immunohistochemistry in tumors of ZH-161-NC or ZH-161-IS glioma-bearing mice 48 h after peg-IFN-β1a treatment in vivo (Figure 2H).

Altered Morphological and Cell Culture Phenotype Upon Chronic IFN-β1a Exposure

During culturing NC and IS cells in parallel, differences in proliferation were observed. While cell-doubling times of NC and IS cells under optimal growth conditions were not different (Figure 3A), sphere formation defined as clusters of more than 5 cells was reduced in IS cells compared with NC cells. Furthermore, sphere formation capacity was reduced in NC cells by IFN-β1a, whereas IFN-β1a had no such effect in IS cells (Figure 3B). A detailed evaluation of the size and morphology of spheres at day 20 revealed that untreated IS cells and IFN-β1a-treated NC cells generated smaller spheres than vehicle-treated NC cells (Supplementary Figure S1B–D). Limiting dilution assays showed that IS cells had a growth disadvantage compared with NC cells (Figure 3C). When comparing cell cycle progression between NC and IS cells, no difference was observed besides an increased fraction of sub-G1 phase cells in IS cells, indicating spontaneous cell death (Figure 3D). We also noted a minor increase in the EC_{50} values for irradiation and TMZ in the IS models; however, given their overall reduced growth rate relative to NC cells, we considered these data difficult to interpret and not indicative of induced cross-resistance. The previously reported sensitization of GIC to irradiation and TMZ was no longer significant, but again this likely resulted mainly from overall reduced growth rates in the IS cultures (data not shown).

In vivo, the proliferation rate determined by Ki-67 labeling was significantly decreased only in peg-IFN-β1a-treated ZH-161-NC tumors, but not in peg-IFN-β1a-treated ZH-161-IS tumors (Figure 3E). Tumor vessel density studies did not show differences between the treatment groups and cell lines (Supplementary Figure S2). To elucidate the impaired growth of IS cells, we investigated whether cell organelles were affected. Endoplasmatic reticula, Golgi apparatus, and mitochondria of NC and IS cells appeared largely similar (Supplementary Figure S3A). Next we determined senescence-associated β-galactosidase activity using irradiation at 20 Gy as a positive control.[36] IS cells uniformly exhibited higher β-galactosidase activity than NC cells (Figure 4A). In contrast, a single exposure to IFN-β did not induce β-galactosidase activity in NC cells (Supplementary Figure S3B).

By electron microscopy, NC cells of ZH-161 and S-24 appeared unremarkable with intact plasma and nuclear membranes, well-separated nucleoli, physiological size, and physiological distribution of mitochondria. Ribosomes were attached to the rough endoplasmatic reticula and numerous circular vesicles were detectable in the cytoplasm (Figure 4B). In contrast, IS cells contained several autophagosomes filled with cellular components surrounded by double membrane layers, demonstrating the typical phenotype of autophagy.[37] GIC-NC were irradiated with 20 Gy as a positive control for senescence. Similar to IS cells, irradiated cells showed abundant autophagosomes and swollen mitochondria (Supplementary Figure S4A). Yet, LC3 immunoblotting did not confirm constitutive activation of autophagy in IS cells (Supplementary Figure S4B), and IS cells were not more sensitive to the inhibition of autophagy by 3-methyladenine than NC cells (Supplementary Figure S4C).

In IS cells, rough endoplasmatic reticula were partially devoid of ribosomes, indicating impaired protein synthesis (Figure 4B). Given this depletion of ribosomes in IS cells, NC cells were also treated with cycloheximide, an inhibitor of protein synthesis. Cycloheximide-treated NC cells showed a different phenotype compared to IS cells, exhibiting substantial amounts of intermediate filaments near the nucleus and mitochondria with dilated cristae and high electron negativity (Supplementary Figure S4D). To gain support for impaired protein synthesis, a protein synthesis assay was performed using cycloheximide-treated NC cells as a positive control. No difference between NC and IS cells became apparent (Supplementary Figure S4E).

Transcriptional Profiling of IS Cells Reveals Downregulation of Gene Sets Related to Receptor Signaling and Cell Migration

Whole-transcriptome sequencing revealed profound changes in the transcriptional landscape in IS cells relative to the corresponding NC controls. Overall, 783 genes were significantly differentially expressed in both IS models versus the respective NC cells. Specifically, 578 and 205 genes were consistently upregulated or downregulated, respectively, in both ZH-161 and S-24 IS cells (Supplementary Table S1, Supplementary Figure S5A). Notably, unsupervised hierarchical clustering using the top 200 (Figure 5A) or all differentially expressed transcripts (Supplementary Figure S5B) clearly segregated the models according to IS versus NC phenotype. Gene set enrichment analysis comparing the transcriptional profiles of both IS models with their NC GIC counterparts revealed upregulation of "interferon signaling" and "negative control of viral process," likely reflecting the direct signaling activity of type I IFN (Figure 5B and C).

Upregulation of the senescence marker, protein tyrosine phosphatase receptor type J,[38] was consistent with the morphological observations in IS cells (Supplementary Figure S5C). In addition, activating transcription factor 4 signaling was upregulated in IS cells compared to NC cells. Although protein kinase RNA–like endoplasmic reticulum kinase (PERK)/eukaryotic translation initiation factor 2-alpha kinase 3 (EIF2AK3) were not differentially regulated between IS and NC cells, EIF2AK2, which is typically upregulated during viral infections, was upregulated in IS cells (Supplementary Figure S5D). Also, genes related to the terms *oxidative phosphorylation* (normalized enrichment score, NES, 1.67, *P*-value 0), *mitochondrial gene*

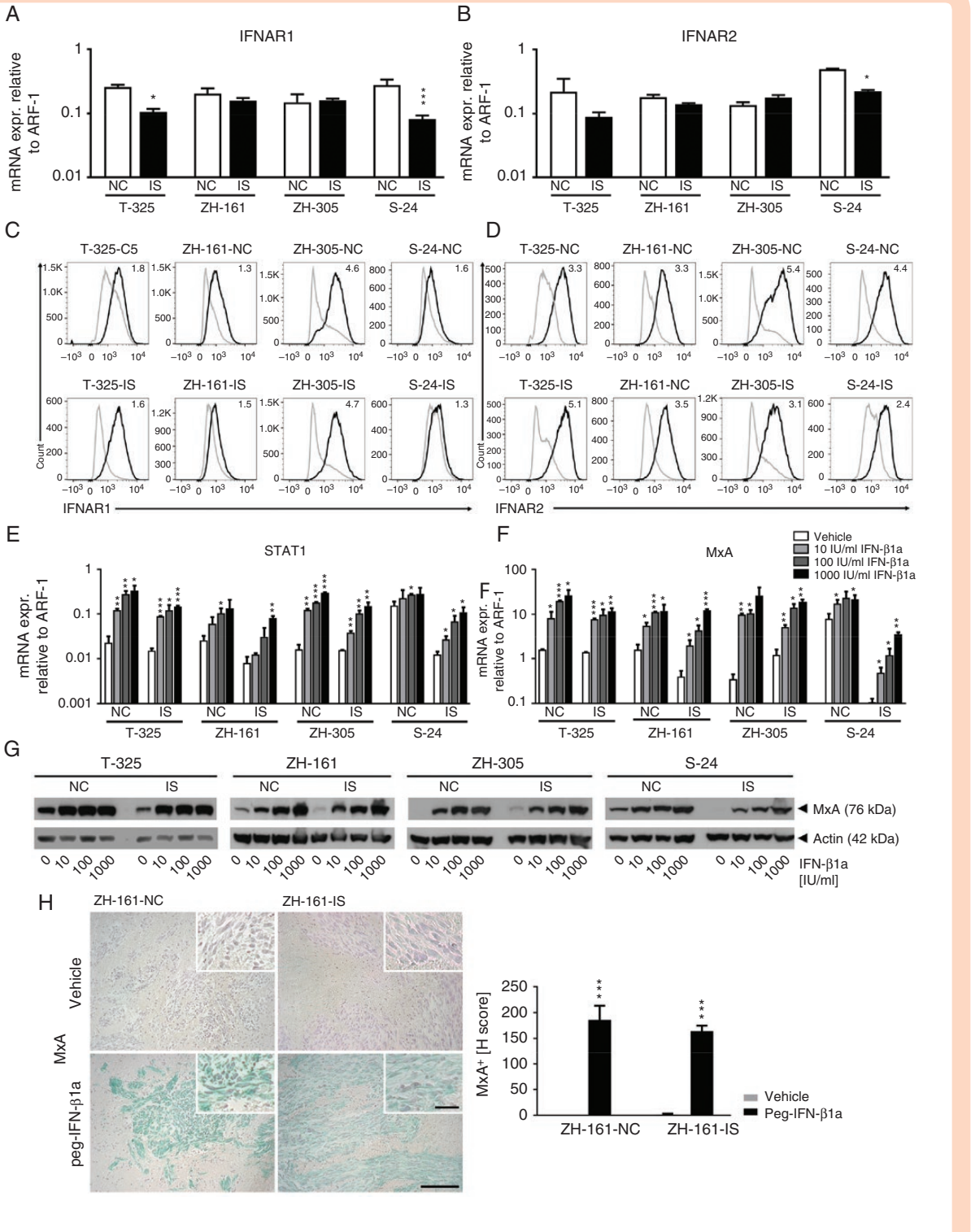

Figure 2. Classical type I IFN signaling in IS versus NC cells in vitro and in vivo. (A–D) NC or IS cells were studied for *IFNAR1* and *IFNAR2* mRNA expression by RT-PCR (A and B). Protein levels of IFNAR1 (C) and IFNAR2 (D) were analyzed by cell surface flow cytometry. Specific fluorescence indexes (SFIs) are indicated in the upper right corner. (E–G) Responsiveness to IFN-β1a (24 h) was assessed at the level of STAT1 (E) and MxA (F) gene expression by RT-PCR and protein accumulation by immunoblot (G). *ARF-1* served as a housekeeping gene for RT-PCR and actin served as a loading control in immunoblots. (H) Brain sections of ZH-161-NC or ZH-161-IS tumor-bearing animals sacrificed when the third mouse became symptomatic were immunohistochemically stained for MxA protein. Data are expressed as mean and SEM (***$P < .001$, one-way ANOVA with Tukey's post hoc test for multiple analysis, peg-IFN-β1a vs vehicle treatment). Scale bars of full pictures correspond to 100 μm, scale bars of inserts to 25 μm.

expression (NES 1.67, *P*-value 0), and *hallmark unfolded protein response* (NES 1.45, *P*-value .009) were positively enriched in IS cells (Supplementary Table S2), but did not pass the false discovery rate threshold to be included in the gene set enrichment analysis.

One candidate gene induced in both IS models, nerve growth factor receptor (*NGFR*), was also induced in 2 other IS models not subjected to gene expression profiling (Supplementary Figure S5E). Notably, the largest cluster downregulated in IS cells contained gene sets involved in receptor signaling. The top-ranking gene set among these affected signaling nodes was *transmembrane receptor protein tyrosine kinase activity* (NES –2.64, false discovery rate *q*-value 4.79 × 10^{-04}). The transmembrane receptor protein tyrosine kinase, anaplastic lymphoma kinase (ALK), was the most significantly downregulated transcript (Supplementary Table S1). The reduction of *ALK* mRNA and protein in IS cells was confirmed by RT-PCR and immunoblot (Supplementary Figure S5F and G). Appropriate control experiments showed that a single exposure of either GIC line to IFN-β was insufficient to reduce *ALK* mRNA expression (data not shown). Hence, loss of ALK signaling activity may mediate part of the resistance to type I IFN.

Another cluster downregulated in IS cells involved cell migration although genes in this cluster overlap with *receptor signaling* cluster. Migration-associated genes downregulated in IS cells included *IFITM1, DDX58*, and *LAMB1* (Figure 6). Accordingly, ZH-161 IS cells formed less invasive tumors than ZH-161 NC cells (Supplementary Figure S6).

Discussion

The present study sought to explore the biological consequences of chronic exposure of human glioblastoma stem cell models to type I IFN signaling. Repeated stimulation of GIC with IFN-β resulted in sublines referred to as IS that were refractory to the inhibitory effects of IFN on stemness defined by a reduction of spherogenicity. IS cells generated by repetitive exposure to IFN-β1a remained insensitive to IFN-β1a-induced suppression of sphere formation for weeks (Figure 1, Supplementary Figure S1A) which could not be attributed to adaptive downregulation of canonical IFN signaling (Figure 2). Resistance to IFN-mediated growth suppression was maintained in vivo while canonical signaling was preserved there, too (Figures 1D and 2).

Cellular unresponsiveness to IFN has previously been analyzed in vitro and in vivo in other cell types. Permanent stimulation with high-dose IFN or long-lasting peg-IFN led to the downregulation of the IFNAR1 cell surface receptor in HEK-293T cells in vitro.[39] The state of unresponsiveness of IFN-treated cells lasted up to 3 days.[40] Once IFN was removed, IFNAR1 cell surface expression returned to control levels within 3 h.[39] In addition, mice repeatedly treated with murine IFN-α became refractory to further IFN injection within hours after the first treatment by upregulating the ubiquitin-specific peptidase 18 (USP18) which has been described as a negative regulator of type I IFN signaling[41] and which was also upregulated in the IS models studied here (Figure 6).

Acquired resistance to IFN-β-induced growth suppression came at a price: the IS phenotype was characterized by decreased constitutive sphere formation, impaired growth under suboptimal conditions, and increased survival of tumor-bearing mice (Figures 1C and 3, Supplementary Figure S1B–D). Possible pathways induced by IFN-β and associated with decreased growth in IS cells include senescence[42] and autophagy[37] (Figure 4). Senescence is a state in which viable cells cease to divide whereas autophagy is a catabolic process that degrades and recycles unnecessary or dysfunctional cellular components inside lysosomes. Both processes can be triggered by cytotoxic stress.[43,44] The phenotype of senescence can be heterogeneous and its expression depends on the exposed stress. It may comprise different effector mechanisms including autophagy, resistance to apoptosis, or activity of cyclin-dependent kinase inhibitors.[45–47] Metabolic or genotoxic stress-induced autophagy can have a survival effect rather than mediating cell death and allow a switch between apoptosis and senescence. Aging fibroblasts revealed some features of the IS phenotype such as increased β-galactosidase activity associated with an increased number of autophagic vacuoles.[48]

Plenty nondistinct fragmented membranes were also observed in IS cells which most likely originate from the rough endoplasmatic reticulum due to their shape and structure. Furthermore, rough endoplasmatic reticula without ribosomes attached were detected. Since ribosomes are associated with the translation of mRNA into protein,[49] this might indicate impaired protein synthesis in IS cells (Figure 4B). When comparing IS cells to NC cells that were treated with CHX as a positive control for inhibited protein synthesis,[50] CHX-treated NC still shared more morphological similarities with untreated NC than with untreated IS cells, suggesting that impaired protein synthesis in IS cells does not go along with morphological changes or that protein synthesis is not affected in IS cells to a relevant quantitative extent (Supplementary Figure S4D). Increased expression of genes related to the unfolded protein response was confirmed by transcriptional profiling (Supplementary Figure S5D and E). RNA sequencing revealed profound changes in IS versus NC cells: maintained signaling activity of type I IFN was confirmed by demonstrating upregulation of genes related to *interferon signaling* and *negative control of viral processes*. In contrast, among multiple gene families downregulated in IS cells, genes related to *tyrosine receptor signaling* and *cell migration* were of particular interest to understand the IS phenotype (Figure 5B). The profound changes in transcriptional profiles raise the possibility of durable epigenetic changes induced by type I IFN.

Altogether, these data indicate that prolonged exposure of human glioblastoma patients to type I IFN at sufficient local concentrations might be a suitable strategy to overcome treatment resistance. Local delivery might be a strategy to achieve this goal while circumventing systemic toxicity. Future studies should explore how to integrate IFN exposure with other novel treatment strategies, notably in the field of immunooncology.

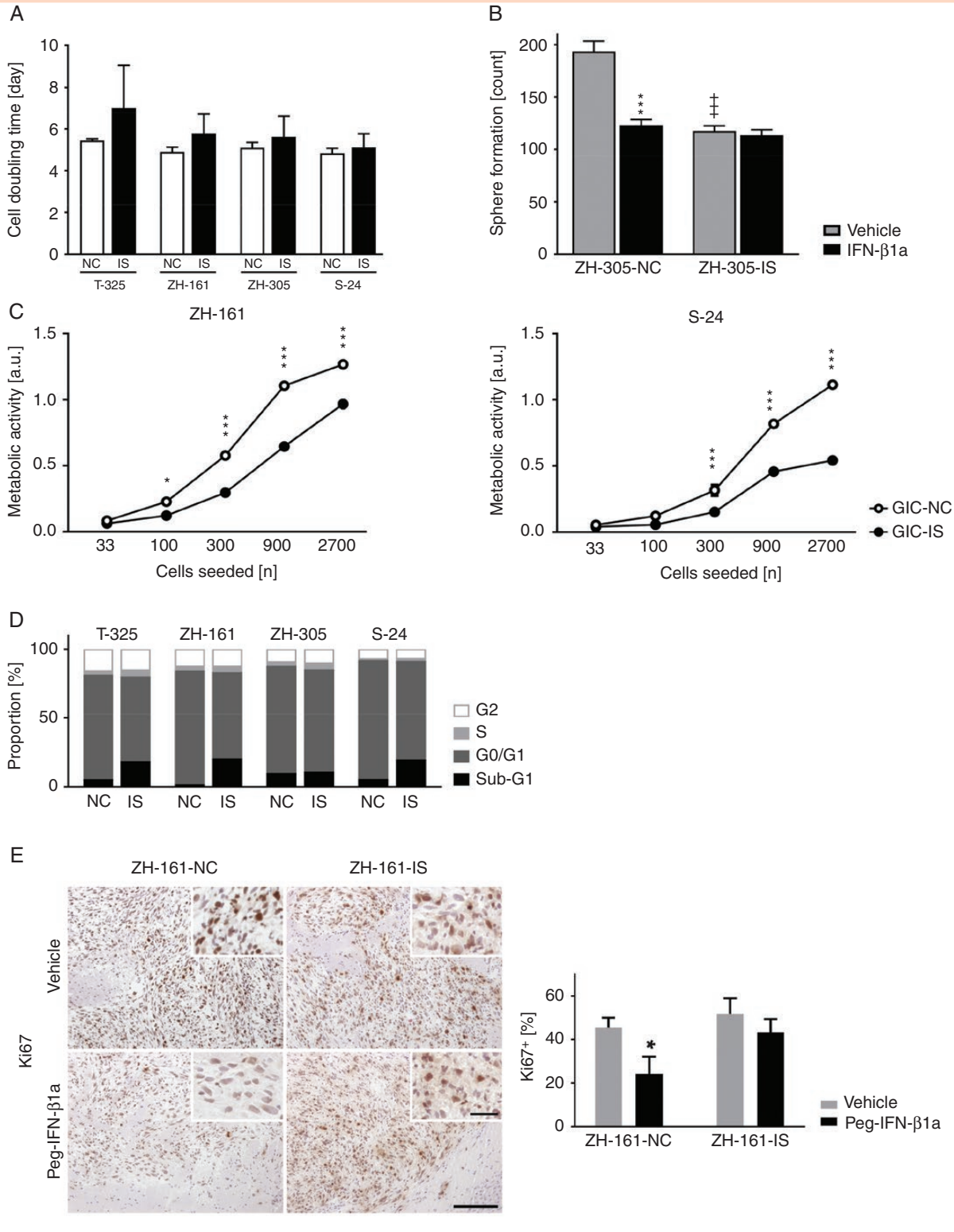

Figure 3. Chronic IFN-β1a exposure induces an altered phenotype in IS cells. (A) Cell doubling times of NC versus IS cells under optimal growth conditions. (B) Responsiveness to IFN-β1a (100 IU/mL) was determined by obtaining sphere counts of ZH-305-NC and ZH-305-IS on day 20. Data are expressed as mean and SEM (one-way ANOVA with Tukey's post hoc test for multiple analysis, $^{***}P < .001$ IFN-β1a-treated vs untreated cells, $^{+++}P < .001$ IS vs NS cells). (C) Sphere formation of ZH-161 and S-24-NC (white) or IS (black) cells after seeding different cell densities. Metabolic activity was assessed by MTT assay. (D) Proportions of cell cycle distribution of NC versus IS cells (black = sub-G1, dark gray = G0/G1, light gray = S, white = G2 phase). (E) Proliferation was analyzed by determining the percentage of Ki-67-positive tumor cell nuclei in ZH-161-NC or ZH-161-IS tumor-bearing mice. Data are expressed as mean and SEM ($^{***}P < .001$, one-way ANOVA with Tukey's post hoc test for multiple analysis, peg-IFN-β1a vs vehicle treatment). Scale bars of full pictures correspond to 100 μm, scale bars of inserts to 25 μm.

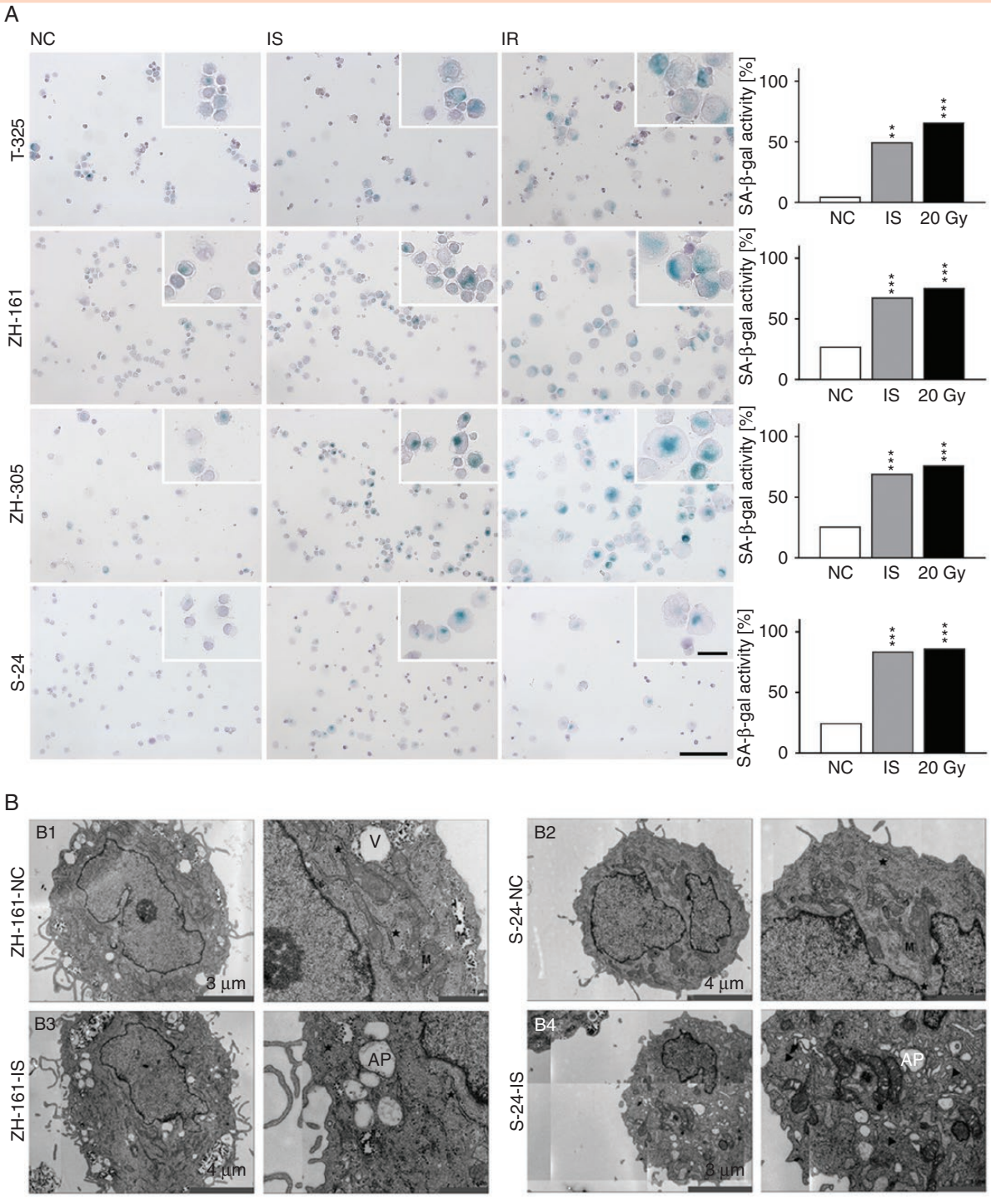

Figure 4. Morphological characteristics of GIC-IS. (A) Senescence-associated β-galactosidase staining on cytospins of untreated NC or IS cells, using irradiated NC cells (20 Gy, 5 days) as a positive control. Scale bars of the full picture correspond to 100 µm, scale bars of insert correspond to 25 µm. Data are expressed as mean percentages and SEM of stained cells (***$P < .001$, one-way ANOVA with Tukey's post hoc test for multiple analysis, IS or irradiated cells vs NC cells). (B) Transmission electron microscopy features of ZH-161 and S-24 NC versus IS cells. Representative pictures of 70 nm sections are shown. V = vesicle (B1), M = mitochondria (B1, B2), asterisk = rough endoplasmatic reticulum (B1–B4), AP = autophagosome (B3, B4), and arrow = nondistinct fragmented membranes (B4).

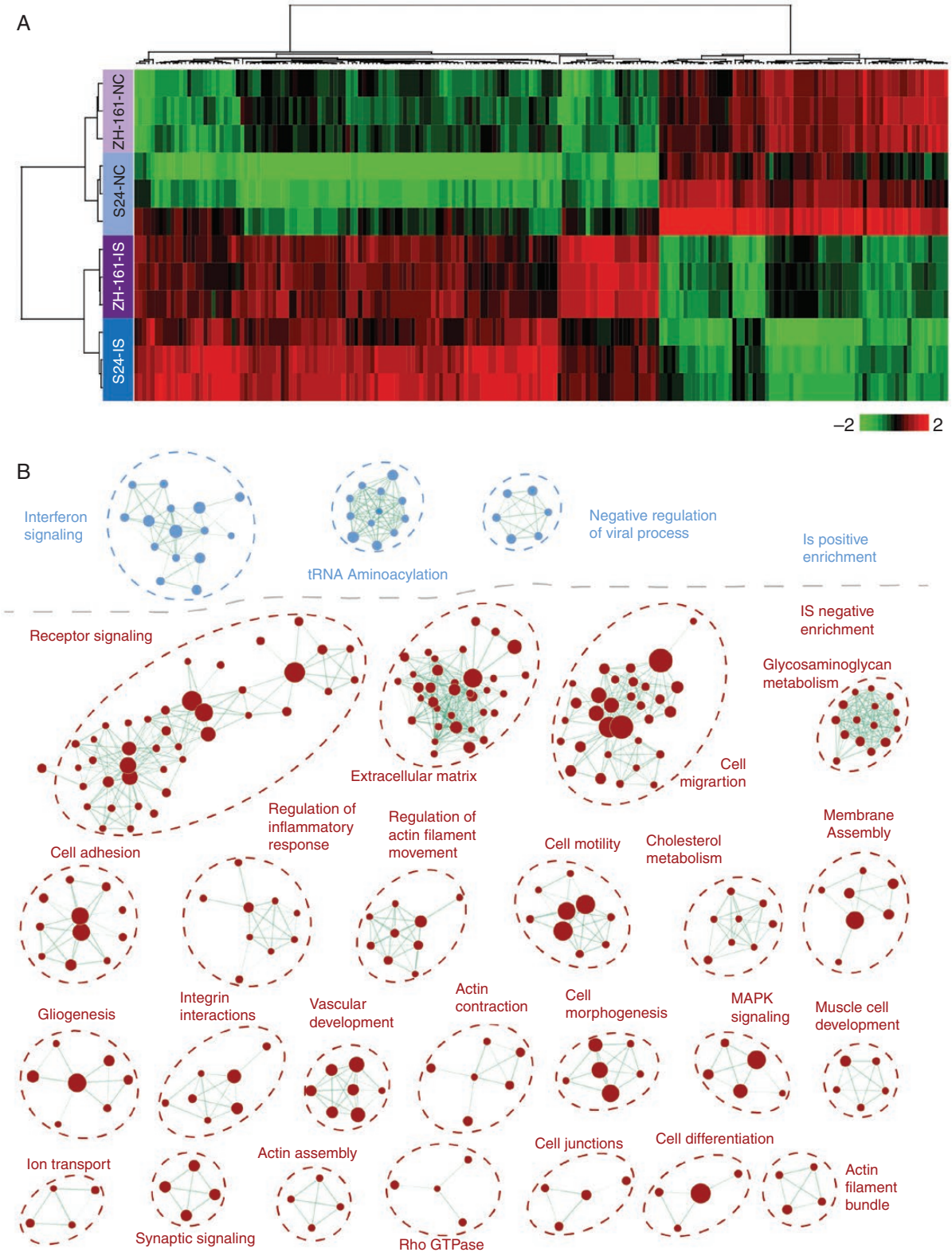

Figure 5. Gene expression profiling of the IS phenotype. (A) Unsupervised hierarchical clustering using the top 200 genes. Upregulated genes are indicated in red, downregulated genes in green (*Z*-score ±2). (B) Visualization of the gene set enrichment analysis of ZH-161 and S-24 IS versus NC cells. Each dot indicates a gene set. Blue dots indicate a positive enrichment in IS cells, and red dots refer to a negative enrichment in IS cells. The size of the dots corresponds to the number of genes present (for details, see Methods).

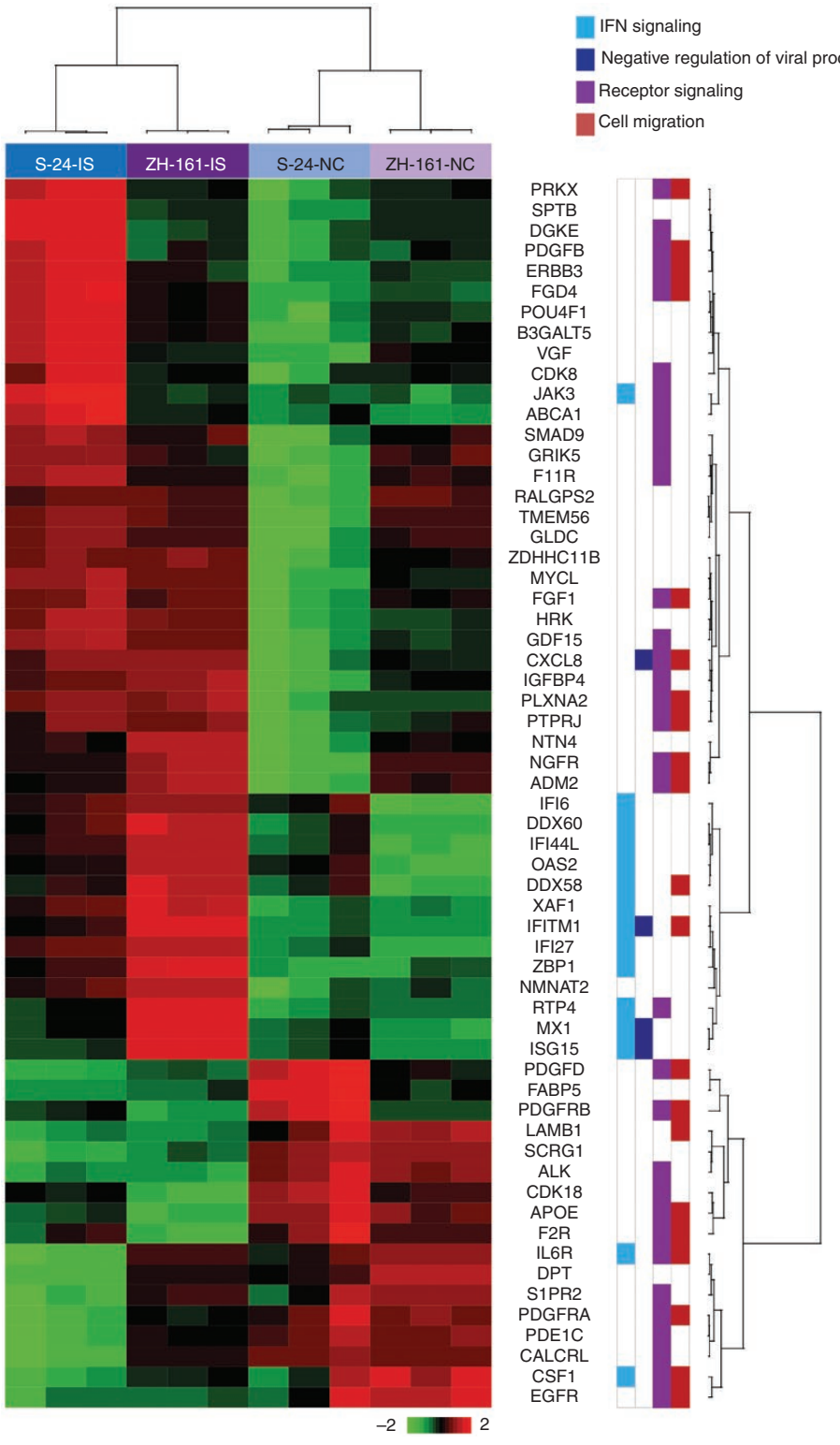

Figure 6. Gene expression profiling of the IS phenotype in both models combined. Unsupervised hierarchical clustering of the most differentially regulated genes in both models combined. Upregulated genes are indicated in red, and downregulated genes in green (*Z*-score ±2). Genes involved in IFN signaling are marked in light blue. Genes associated with negative regulation of viral processes are labeled in dark blue. Genes referring to cell migration are indicated in purple.

Supplementary Data

Supplementary data are available at *Neuro-Oncology Advances* online.

Keywords

glioblastoma | interferon | signaling | stemness | transcription.

Funding

This study was supported by the Swiss National Science Foundation [310030_166634/1, 310030_185155/1]; a joint grant from the Deutsche Forschungsgemeinschaft (DFG) and the Swiss National Science Foundation to M.R., G.R., P.R., and M.W. [RE 2857/2-1, RE938/4-1; 310030E_170717]; and a research grant of Biogen (Cambridge, MA) to M.W.

Acknowledgments

The authors thank D. Baker and M. Naylor (both from Biogen) for valuable discussions and J. Friesen and F. Wiget for expert technical assistance.

Conflicts of interest statement: B.L., M.S., D.P., H.S., and M.R. report no conflicts of interest. P.R. has received research support from MSD and honoraria for advisory board participation or lectures from Bristol-Myers Squibb, Covagen, Medac, MSD, Novocure, Roche, and Virometix. G.R. has received research grants from Roche and Merck as well as honoraria for advisory boards from Abbvie. M.W. has received research grants from Abbvie, Adastra, Dracen, Merck, Sharp & Dohme (MSD), Merck (EMD), Novocure, Piqur, and Roche and honoraria for lectures or advisory board participation or consulting from Abbvie, Basilea, Bristol Meyer Squibb (BMS), Celgene, Merck, Sharp & Dohme (MSD), Merck (EMD), Novocure, Orbus, Roche, and Tocagen.

Authorship Statement

Experimental design and implementation (B.L., H.S., and M.W.), analysis and interpretation of the data (B.L., M.S., D.P., H.S., M.R., P.R., and G.R.), and writing of the manuscript (M.W.).

References

1. Louis DN, Perry A, Reifenberger G, et al. The 2016 World Health Organization Classification of Tumors of the Central Nervous System: a summary. *Acta Neuropathol.* 2016;131(6):803–820.
2. Gramatzki D, Dehler S, Rushing EJ, et al. Glioblastoma in the Canton of Zurich, Switzerland revisited: 2005 to 2009. *Cancer.* 2016;122(14):2206–2215.
3. Ostrom QT, Gittleman H, Liao P, et al. CBTRUS Statistical Report: primary brain and other central nervous system tumors diagnosed in the United States in 2010–2014. *Neuro Oncol.* 2017;19(Suppl 5):v1–v88.
4. Chinot OL, Wick W, Mason W, et al. Bevacizumab plus radiotherapy-temozolomide for newly diagnosed glioblastoma. *N Engl J Med.* 2014;370(8):709–722.
5. Gilbert MR, Dignam JJ, Armstrong TS, et al. A randomized trial of bevacizumab for newly diagnosed glioblastoma. *N Engl J Med.* 2014;370(8):699–708.
6. Weller M, Butowski N, Tran DD, et al.; ACT IV Trial Investigators. Rindopepimut with temozolomide for patients with newly diagnosed, EGFRvIII-expressing glioblastoma (ACT IV): a randomised, double-blind, international phase 3 trial. *Lancet Oncol.* 2017;18(10):1373–1385.
7. Weller M, van den Bent M, Tonn JC, et al.; European Association for Neuro-Oncology (EANO) Task Force on Gliomas. European Association for Neuro-Oncology (EANO) guideline on the diagnosis and treatment of adult astrocytic and oligodendroglial gliomas. *Lancet Oncol.* 2017;18(6):e315–e329.
8. Stupp R, Mason WP, van den Bent MJ, et al.; European Organisation for Research and Treatment of Cancer Brain Tumor and Radiotherapy Groups; National Cancer Institute of Canada Clinical Trials Group. Radiotherapy plus concomitant and adjuvant temozolomide for glioblastoma. *N Engl J Med.* 2005;352(10):987–996.
9. Hegi ME, Diserens AC, Gorlia T, et al. MGMT gene silencing and benefit from temozolomide in glioblastoma. *N Engl J Med.* 2005;352(10):997–1003.
10. Hegi ME, Genbrugge E, Gorlia T, et al. MGMT promoter methylation cutoff with safety margin for selecting glioblastoma patients into trials omitting temozolomide. A pooled analysis of four clinical trials. *Clin Cancer Res.* 2018;25(6):1809–1816.
11. Happold C, Roth P, Silginer M, et al. Interferon-β induces loss of spherogenicity and overcomes therapy resistance of glioblastoma stem cells. *Mol Cancer Ther.* 2014;13(4):948–961.
12. Natsume A, Ishii D, Wakabayashi T, et al. IFN-beta down-regulates the expression of DNA repair gene MGMT and sensitizes resistant glioma cells to temozolomide. *Cancer Res.* 2005;65(17):7573–7579.
13. Platanias LC. Mechanisms of type-I- and type-II-interferon-mediated signalling. *Nat Rev Immunol.* 2005;5(5):375–386.
14. Pestka S, Krause CD, Walter MR. Interferons, interferon-like cytokines, and their receptors. *Immunol Rev.* 2004;202:8–32.
15. Trinchieri G. Type I interferon: friend or foe? *J Exp Med.* 2010;207(10):2053–2063.
16. Zitvogel L, Galluzzi L, Kepp O, Smyth MJ, Kroemer G. Type I interferons in anticancer immunity. *Nat Rev Immunol.* 2015;15(7):405–414.
17. Dunn GP, Bruce AT, Sheehan KC, et al. A critical function for type I interferons in cancer immunoediting. *Nat Immunol.* 2005;6(7):722–729.
18. Koebel CM, Vermi W, Swann JB, et al. Adaptive immunity maintains occult cancer in an equilibrium state. *Nature.* 2007;450(7171):903–907.
19. Schreiber RD, Old LJ, Smyth MJ. Cancer immunoediting: integrating immunity's roles in cancer suppression and promotion. *Science.* 2011;331(6024):1565–1570.
20. Kayo H, Yamazaki H, Nishida H, Dang NH, Morimoto C. Stem cell properties and the side population cells as a target for interferon-alpha in adult T-cell leukemia/lymphoma. *Biochem Biophys Res Commun.* 2007;364(4):808–814.
21. Moserle L, Indraccolo S, Ghisi M, et al. The side population of ovarian cancer cells is a primary target of IFN-alpha antitumor effects. *Cancer Res.* 2008;68(14):5658–5668.

22. Régnier-Rosencher E, Guillot B, Dupin N. Treatments for classic Kaposi sarcoma: a systematic review of the literature. *J Am Acad Dermatol.* 2013;68(2):313–331.
23. Maevis V, Mey U, Schmidt-Wolf G, Schmidt-Wolf IG. Hairy cell leukemia: short review, today's recommendations and outlook. *Blood Cancer J.* 2014;4:e184.
24. Quesada JR, Reuben J, Manning JT, Hersh EM, Gutterman JU. Alpha interferon for induction of remission in hairy-cell leukemia. *N Engl J Med.* 1984;310(1):15–18.
25. Flanigan RC, Salmon SE, Blumenstein BA, et al. Nephrectomy followed by interferon alfa-2b compared with interferon alfa-2b alone for metastatic renal-cell cancer. *N Engl J Med.* 2001;345(23):1655–1659.
26. Talpaz M, Kantarjian HM, McCredie K, Trujillo JM, Keating MJ, Gutterman JU. Hematologic remission and cytogenetic improvement induced by recombinant human interferon alpha A in chronic myelogenous leukemia. *N Engl J Med.* 1986;314(17):1065–1069.
27. Mandelli F, Avvisati G, Amadori S, et al. Maintenance treatment with recombinant interferon alfa-2b in patients with multiple myeloma responding to conventional induction chemotherapy. *N Engl J Med.* 1990;322(20):1430–1434.
28. Mellstedt H, Aahre A, Bjørkholm M, et al. Interferon therapy in myelomatosis. *Lancet.* 1979;2(8144):697.
29. Groves MD, Puduvalli VK, Gilbert MR, et al. Two phase II trials of temozolomide with interferon-alpha2b (pegylated and non-pegylated) in patients with recurrent glioblastoma multiforme. *Br J Cancer.* 2009;101(4):615–620.
30. Motomura K, Natsume A, Kishida Y, et al. Benefits of interferon-β and temozolomide combination therapy for newly diagnosed primary glioblastoma with the unmethylated MGMT promoter: a multicenter study. *Cancer.* 2011;117(8):1721–1730.
31. Wakabayashi T, Kayama T, Nishikawa R, et al. A multicenter phase I trial of combination therapy with interferon-β and temozolomide for high-grade gliomas (INTEGRA study): the final report. *J Neurooncol.* 2011;104(2):573–577.
32. Wakabayashi T, Natsume A, Mizusawa J, et al.; Members of Japan Clinical Oncology Group Brain Tumor Study Group (JCOG-BTSG). JCOG0911 INTEGRA study: a randomized screening phase II trial of interferonβ plus temozolomide in comparison with temozolomide alone for newly diagnosed glioblastoma. *J Neurooncol.* 2018;138(3):627–636.
33. Happold C, Roth P, Wick W, et al. Distinct molecular mechanisms of acquired resistance to temozolomide in glioblastoma cells. *J Neurochem.* 2012;122(2):444–455.
34. Le Rhun E, von Achenbach C, Lohmann B, et al. Profound, durable and MGMT-independent sensitivity of glioblastoma cells to cyclin-dependent kinase inhibition. *Int J Cancer.* 2018;145(1):242–253.
35. Schneider H, Lohmann B, Wirsching HG, et al. Age-associated and therapy-induced alterations in the cellular microenvironment of experimental gliomas. *Oncotarget.* 2017;8(50):87124–87135.
36. Fumagalli M, Rossiello F, Mondello C, d'Adda di Fagagna F. Stable cellular senescence is associated with persistent DDR activation. *PLoS One.* 2014;9(10):e110969.
37. Boya P, Codogno P, Rodriguez-Muela N. Autophagy in stem cells: repair, remodelling and metabolic reprogramming. *Development.* 2018;145(4).
38. Althubiti M, Lezina L, Carrera S, et al. Characterization of novel markers of senescence and their prognostic potential in cancer. *Cell Death Dis.* 2014;5:e1528.
39. Marijanovic Z, Ragimbeau J, Kumar KG, Fuchs SY, Pellegrini S. TYK2 activity promotes ligand-induced IFNAR1 proteolysis. *Biochem J.* 2006;397(1):31–38.
40. Larner AC, Chaudhuri A, Darnell JE Jr. Transcriptional induction by interferon. New protein(s) determine the extent and length of the induction. *J Biol Chem.* 1986;261(1):453–459.
41. Sarasin-Filipowicz M, Wang X, Yan M, et al. Alpha interferon induces long-lasting refractoriness of JAK-STAT signaling in the mouse liver through induction of USP18/UBP43. *Mol Cell Biol.* 2009;29(17):4841–4851.
42. Lee BY, Han JA, Im JS, et al. Senescence-associated beta-galactosidase is lysosomal beta-galactosidase. *Aging Cell.* 2006;5(2):187–195.
43. Serrano M, Lin AW, McCurrach ME, Beach D, Lowe SW. Oncogenic ras provokes premature cell senescence associated with accumulation of p53 and p16INK4a. *Cell.* 1997;88(5):593–602.
44. Young AR, Narita M. Connecting autophagy to senescence in pathophysiology. *Curr Opin Cell Biol.* 2010;22(2):234–240.
45. Hernandez-Segura A, Nehme J, Demaria M. Hallmarks of cellular senescence. *Trends Cell Biol.* 2018;28(6):436–453.
46. Patschan S, Chen J, Polotskaia A, et al. Lipid mediators of autophagy in stress-induced premature senescence of endothelial cells. *Am J Physiol Heart Circ Physiol.* 2008;294(3):H1119–H1129.
47. Young AR, Narita M, Ferreira M, et al. Autophagy mediates the mitotic senescence transition. *Genes Dev.* 2009;23(7):798–803.
48. Gerland LM, Peyrol S, Lallemand C, Branche R, Magaud JP, Ffrench M. Association of increased autophagic inclusions labeled for beta-galactosidase with fibroblastic aging. *Exp Gerontol.* 2003;38(8):887–895.
49. Savir Y, Tlusty T. The ribosome as an optimal decoder: a lesson in molecular recognition. *Cell.* 2013;153(2):471–479.
50. Roth W, Fontana A, Trepel M, Reed JC, Dichgans J, Weller M. Immunochemotherapy of malignant glioma: synergistic activity of CD95 ligand and chemotherapeutics. *Cancer Immunol Immunother.* 1997;44(1):55–63.